Copper-oxo Active Sites in the 8MR of Zeolite Mordenite: DFT Investigation of the Impact of Acid Sites on Methanol Yield and Selectivity

Olabisi Suleiman[#], Olajumoke Adeyiga[#], Dipak Panthi, and Samuel O. Odoh*
Department of Chemistry, University of Nevada Reno, 1664 N. Virginia Street, Reno, NV 89557-0216

Email Addresses:
sodoh@unr.edu

ABSTRACT: There is significant interest in improving methanol yields from methane in copper-exchanged zeolites. Interestingly, zeolites with proton, H^+, precursors provide greater methanol yields and selectivities than zeolites from sodium, Na^+, precursors. There is however no quantitative description of the origins of these differences. Here, we use density functional theory, DFT, to probe differences in the properties of copper-oxo species in the 8MR of zeolite mordenite, MOR. We focus only on $[Cu_3O_3]^{2+}$, $[Cu_2O]^{2+}$ and two $[Cu_2O_2]^{2+}$ species in H-MOR and Na-MOR. Our calculation show that these sites are activated at 345-490 °C, with the bis(μ-oxo) dicopper (III) $[Cu_2O_2]^{2+}$ moiety being most stable and $[Cu_3O_3]^{2+}$ least stable. $[Cu_3O_3]^{2+}$ and $[Cu_2O]^{2+}$ are capable of activating methane at 200 °C, with similar C-H activation barriers in H-MOR and Na-MOR zeolites. The fate of the methyl group formed from methane C-H activation differentiates the Na-MOR and H-MOR zeolites. Crucially, we show that rebound of the methyl group to an active-site μ-oxo atom favors over-oxidation. Alternatively, the methyl group can be stabilized via exchange with H^+/Na^+ located at remote aluminates. Exchange with Na^+ does not provide as much stabilization as the μ-(O-CH_3) intermediate, thus favoring over-oxidation. By contrast, Brønsted acid sites provide similar levels of stabilization as the μ-(OCH_3) intermediate. This is a path to methanol, rather than over-oxidation products. The discrepancy in the stabilizations provided by Na^+ and H^+-aluminate sites is rooted in the electronic structure.

Keywords: Copper-Exchanged Zeolites, Cu-MOR, Brønsted acid sites, Methane Activation, C-H bond activation, Methanol, Sodium

1. INTRODUCTION

Natural gas is found in large quantities in deposits across the globe. These deposits are often found in remote locations, far removed from urban centers. Thus, natural gas is transported over great distances to locations where it can be used to generate heat, energy and intermediate industrial chemicals.[1-4] As natural gas is a low-density gas, its transportation and storage require significant economical and infrastructure investments. There is therefore strong interest in the development of cheap and efficient platforms for direct conversion of methane to methanol. Direct conversion to methanol is considered an alternative to current technologies utilizing synthesis gas to produce methanol. Direct conversion to methanol is also feasible in small-scale facilities near natural gas deposits, thus limiting the harmful practice of flaring. Interestingly, direct methane-to-methanol conversion (MMC) can be achieved under moderate conditions with copper-exchanged zeolites.[5-10] These zeolites are often useful for MMC in a stepwise manner involving successive active-site formation, methane C-H activation and product desorption steps, followed by regeneration of the copper-oxo active sites. When used in this manner, they can activate methane with very high methanol selectivities, under mild temperature conditions. Moreover, there is great interest in determining the natures of the copper-oxo active site clusters responsible for methane activation in these zeolites.[10,11] Many previous studies sought to provide insights for guided optimization and improvement of the performance of copper-exchanged zeolites.

Interestingly, it has been reported that the topology and composition of the zeolite significantly affect methanol yields. Of particular importance to the current work are observations showing that proton-form precursors lead to copper-exchanged zeolites (H-form zeolites) that yield higher amounts of methanol than those from sodium-form precursors (Na-form zeolites). Dyballa et al. reported that copper-exchanged proton-form mordenite (H-MOR) has significantly higher methanol yields than Na-MOR analogues with similar Si/Al ratios.[12] Methanol yields of H-MOR zeolites were also independent of Si/Al ratios. By contrast, methanol yields from Na-MOR zeolites depend greatly on the Si/Al ratios. These findings for the MOR zeolite agree quite well with the earlier reports by Grundner et al.[13,14] Narsimhan et al. have reported that H-form zeolites also outperform Na-form analogues for steady-state catalytic MMC.[15] They speculated that acid sites in the H-form zeolites might change the energetics of formation of the active sites. More recently, Sushkevich et al. reported that the productivity of Cu-(Na,H)-MOR for methane oxidation is correlated to the amount of Brønsted acid sites (BASs).[16] Specifically, samples with more BASs

provided higher methanol yields and selectivities. Higher BAS concentrations led to lower amounts of over-oxidation products like CO_2. They noted that the BASs play a key role in stabilizing the intermediate species formed from methane activation. Indeed, Park et al. reported similar findings for several framework topologies.[17] Dyballa et al. explicitly linked the acid sites with formation of extra-framework aluminum species.[12] They found that counter-ions like Na^+ stabilize the framework preventing formation of these extra-framework aluminum species.

Improved methane transformation activity of H-form zeolites, relative to Na-form analogues, extend beyond MMC. Narsimhan et al. examined the methane activation-carbonylation reaction over Cu-ZSM-5 to yield methanol and acetic acid. The methanol to acetic acid ratio produced by Cu-H-ZSM-5 is higher than for Cu-Na-ZSM-5.[18] The methoxy species produced in Cu-H-ZSM-5 are active for both oxidation and carbonylation while those in Cu-Na-ZSM-5 are carbonylation inactive.

Despite these observations, quantitative explanations of their origins are rather rare. Grundner et al. previously proposed that the sodium cation, Na^+, competes with divalent copper ions, Cu^{2+}, for framework aluminate tetrahedra.[13] This suggests that Na^+ in the Na-MOR system could prevent siting of copper-oxo active site clusters in the zeolite framework. In this case, the presence of Na^+ or H^+ counter-ions will influence methanol yields by affecting the population distributions of copper-oxo clusters. However, it is also quite possible that these counter-ions could modify active site reactivities, rather than the distributions of the copper-oxo species. Lastly, a combination of these two factors could cause improved methanol yields and selectivities in proton-form zeolites.

In this work, we aim to provide a quantitative assessment of the differences between copper-exchanged zeolites with Na^+ or H^+ counter-ions in the framework. We chose MOR as our model system and thus compared copper-exchanged H-MOR and Na-MOR. All our work was performed with density functional theory, DFT, calculations. Rather than focusing on one copper-oxo cluster, we considered four species: $[Cu_3O_3]^{2+}$, $[Cu_2O]^{2+}$ and two $[Cu_2O_2]^{2+}$ species, all within the 8MR of MOR. These are shown in Figure 1. We sought to provide quantitative answers to these questions:

1) How do H^+ and Na^+ counter-ions influence the structural and electronic structure properties of copper-oxo clusters in the 8MR of zeolite MOR?
2) Do H^+ and Na^+ counter-ions influence the distribution of the copper-oxo sites in MOR? To answer this question, we computed the activation temperatures of copper-oxo sites. We did this by computing the temperature-dependent formation free-energies of the active sites.

3) How do counter-ions affect the activation of a methane C-H bond? We probe this by investigating the methane activation pathways in H-MOR and Na-MOR.
4) What is the fate of the methyl group formed after methane C-H activation? To this end, we examined possible stabilizations of this methyl group in H-MOR and Na-MOR zeolites.

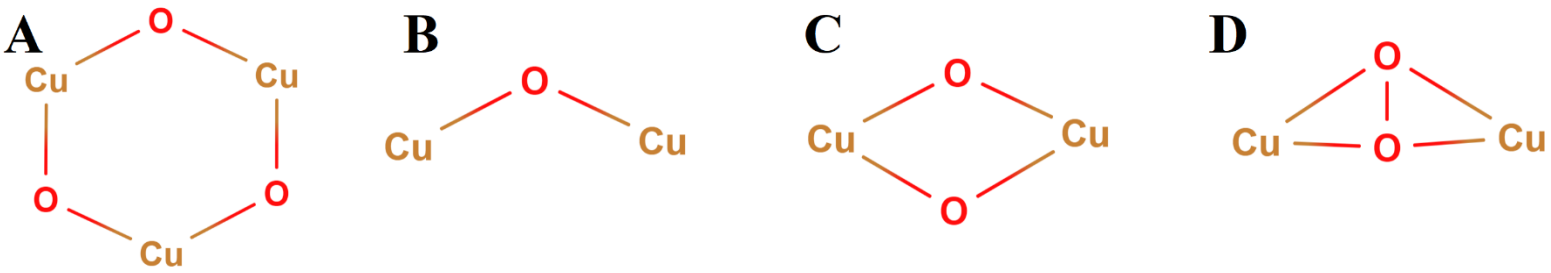

Figure 1: Structures of copper-oxo active sites. **A)** $[Cu_3O_3]^{2+}$, **B)** $[Cu_2O]^{2+}$, **C)** Bis(μ-oxo) dicopper (III) $[Cu_2O_2]^{2+}$ and **D)** bent μ-(η^2:η^2) peroxo dicopper (II) $[Cu_2O_2]^{2+}$.

2. COMPUTATIONAL DETAILS

2.1. Systems of Interest: The unit cell of the proton-form of zeolite mordenite, H_4MOR, Figure 2, was initially optimized. All other structures were created from this. In H_4MOR, the charges of

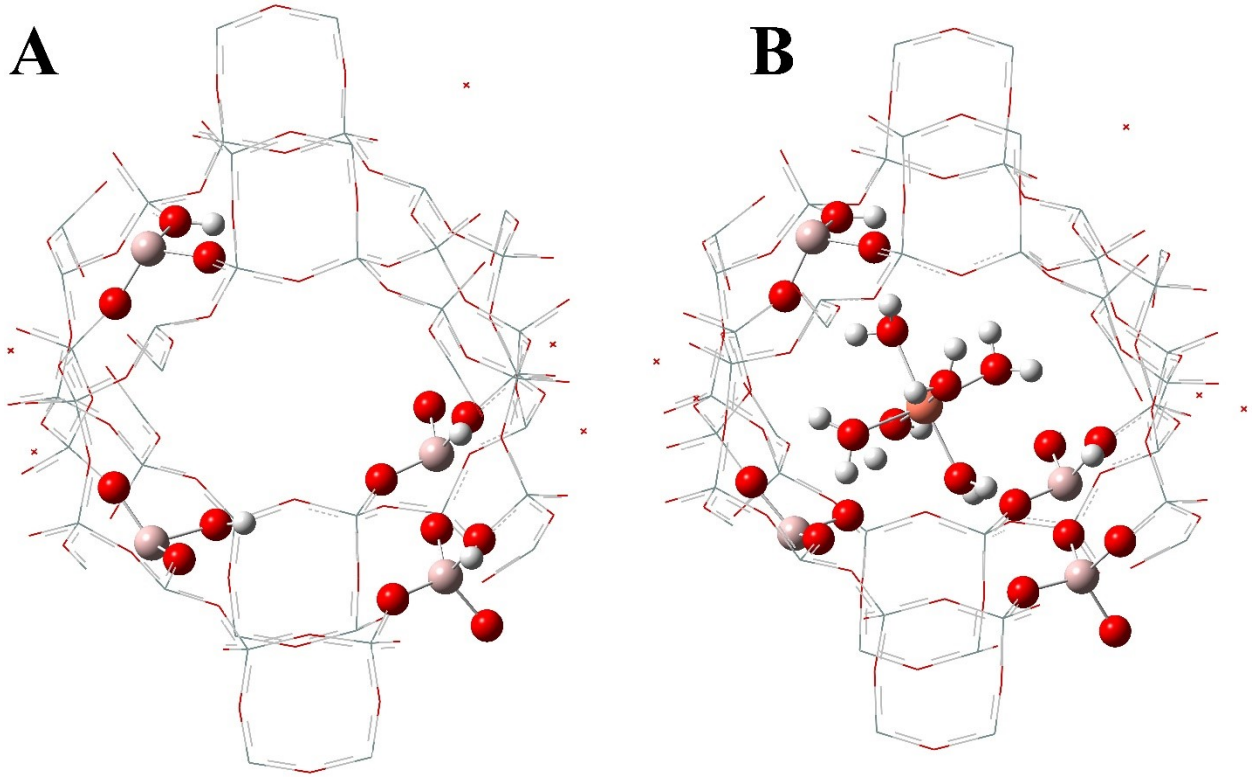

Figure 2: Structures of **A)** H_4MOR and **B)** $[Cu(H_2O)_6](H_2MOR)$. Portions of the zeolite are depicted with wireframes to improve visibility. H, O, Al and Cu atoms are represented with white, red, light pink and brown spheres, respectively.

four aluminate tetrahedra are balanced with protons. This system has a Si/Al ratio of 11/1, consistent with other reports.[13,19] The protons were replaced with Na^+, to form Na_4MOR.

Prior to methane C-H activation, copper species are introduced into the zeolite, generally via ion-exchange with H^+ or Na^+. Under aqueous conditions, the starting species for this exchange is hexaaquo Cu^{2+} ion, $[Cu(H_2O)_6]^{2+}$. To describe the formation of copper-oxo species in MOR, we started from $[Cu(H_2O)_6](H_2MOR)$ and $[Cu(H_2O)_6](Na_2MOR)$, where we have replaced 2 main-channel cations with $[Cu(H_2O)_6]^{2+}$, Figure 2. Dehydration and oxidation of these $[Cu(H_2O)_6]^{2+}$ species leads to the copper-oxo species of interest. These are $[Cu_3O_3]^{2+}$, $[Cu_2O]^{2+}$, bis(μ-oxo) dicopper (III) and bent μ-(η^2:η^2) peroxo dicopper (II) $[Cu_2O_2]^{2+}$, Figure 1.

2.2. Geometry Optimizations: Geometry optimizations were performed with Quantum Espresso[20,21] while using the PBE-D3 functional.[22,23] Convergence thresholds for the self-consistent energies and forces were set to 1×10^{-6} and 1×10^{-3}, respectively. We employed the recommended projected augmented wave (PAW) pseudopotentials with charge density and wavefunction cut-offs set to 350.0 Ry and 50.0 Ry respectively. Sampling of the Brillouin zone was set to the Γ point. This protocol is accurate for studying reactions involved in MMC.

2.3. Single-Point Calculations of Atomic Charges: Single-point calculations on the optimized periodic structures from Quantum-Espresso were performed with the CP2K/Quickstep package[24-26] while also using the PBE-D3 functional. We used triple-ζ TZVP-MOLOPT-SR-GTH basis sets, optimized for computing molecular properties.[27] These basis sets were used along with PBE-GTH Goedecker-Teter-Hutter pseudopotentials and a 1200 Ry plane-wave cutoff.[28-30] All calculations were performed at the Γ point. We computed the Hirshfeld atomic partial charges.[31]

2.4. Transition State Searches: The pathway for reaction of the copper-oxo sites with methane for C-H were investigated with the nudged-elastic band, NEB, method.[32,33] We used the optimized MOR cells and 5-10 images between the reactants and products for the C-H activation step. We also ensured that all translations and rotations were frozen out from the starting coordinates. The simulations were stopped when the norm of the force orthogonal to the reaction path was less than 0.05 eV/Å.

2.5. Vibrational Frequency Analysis: In order to obtain reaction free-energies, some systems were re-optimized with the periodic DFT NWPW module of the NWChem software.[34] Vibrational frequency analysis were performed with the harmonic approximation while still using the PBE-

D3 density functional. The wavefunction cutoff was set to 140 Ry and the cutoff energy for the density was set to 280 Ry. Further details are provided in the Supporting Information.

3. RESULTS AND DISCUSSIONS

3.1. Structural and Electronic Properties of Zeolites and Active Sites

In this section, we compare the electronic structures and geometrical properties of various H-MOR and Na-MOR zeolites. We first compare the properties of the precursor zeolites, H_4MOR and Na_4MOR. These are the species without any copper-oxo cluster. We then compare the properties of copper-exchanged zeolites, in which two counter-ions are replaced with $[Cu_3O_3]^{2+}$, $[Cu_2O]^{2+}$ or the $[Cu_2O_2]^{2+}$ species.

3.1.1. Electronic properties of precursor zeolites: The structures of H_4MOR and Na_4MOR are shown in Figure 2. The average distance between H^+ and Na^+ counter-ions to the nearest aluminate oxo atom are 0.995 and 2.319 Å, respectively. This is as expected, considering the radii of the H and Na atoms. However, the sum of the Hirshfeld partial atomic charges on the protons in H_4MOR is 1.49, Table 1. In Na_4MOR, the Hirshfeld charges on the Na atoms sum up to 2.11. Thus, the MOR framework has a net charge of -1.49 in H_4MOR and -2.11 for Na_4MOR. This indicates greater charge separation between the framework and counter-cations in Na_4MOR. Based on this, we conclude that Na_4MOR's framework will favor interaction with highly ionic species.

Table 1: Hirshfeld charges on the framework, active site motif and charge-balancing ions in several species.

	Precursor Zeolites		$[Cu_3O_3]^{2+}$ species		$[Cu_2O]^{2+}$ species	
	H_4MOR	Na_4MOR	H-MOR	Na-MOR	H-MOR	Na-MOR
Framework	-1.49	-2.11	-1.32	-1.58	-1.52	-1.74
Active site			+0.57	+0.53	+0.70	+0.69
Counter-cation	+1.49	+2.11	+0.75	+1.05	+0.82	+1.05
			Bis(μ-oxo) $[Cu_2O_2]^{2+}$ species		Peroxo $[Cu_2O_2]^{2+}$ species	
			H-MOR	Na-MOR	H-MOR	Na-MOR
Framework			-1.33	-1.56	-1.54	-1.77
Active site			+0.51	+0.50	+0.73	+0.72
Counter-cation			+0.82	+1.06	+0.82	+1.05

3.1.2. Electronic properties of activated copper-exchanged zeolites: The copper-exchanged zeolites are $[Cu_2O](H_2MOR)$ and $[Cu_3O_3](H_2MOR)$ as well as their Na-MOR analogues, $[Cu_2O](Na_2MOR)$ and $[Cu_3O_3](Na_2MOR)$. We also considered species with $[Cu_2O_2]^{2+}$ active

sites. For $[Cu_3O_3](H_2MOR)$, the overall charge of the framework is -1.32. The framework is more nucleophilic in $[Cu_3O_3](Na_2MOR)$, with a charge of -1.58. A similar trend exists in the $[Cu_2O]^{2+}$ and $[Cu_2O_2]^{2+}$ species. As an example, in $[Cu_2O](H_2MOR)$ and $[Cu_2O](Na_2MOR)$, the charges on the framework are -1.52 and -1.74, respectively. This represents a 14-20% increase in the framework's nucleophilicity on moving from H-MOR framework to Na-MOR. Thus, the framework in copper-exchanged Na-MOR zeolites will favor interaction with highly ionic species.

Table 2: Hirshfeld spin densities on the Cu and O atoms of several species.

	$[Cu_3O_3]^{2+}$ species		$[Cu_2O]^{2+}$ species	
	H-MOR	Na-MOR	H-MOR	Na-MOR
Cu	0.62, -0.15, -0.30	0.45, 0.27, -0.05	0.60, -0.60	0.59, -0.60
O	0.43, 0.41, -0.02	0.22, 0.10, -0.07	0.00	0.03
	Bis(μ-oxo) $[Cu_2O_2]^{2+}$ species		Peroxo $[Cu_2O_2]^{2+}$ species	
	H-MOR	Na-MOR	H-MOR	Na-MOR
Cu	0.00, 0.00	0.00, 0.00	0.53, -0.53	0.53, -0.54
O	0.00, 0.00	0.00, 0.00	0.00, 0.00	0.00, 0.00

The calculated Hirshfeld spin densities on the Cu and O atoms of the copper-oxo active site clusters are presented in Table 2. For the dicopper species, the spin densities are mostly the same in the H-form and Na-form zeolites. Indeed, in the dicopper species, the μ-oxo atoms are all of oxo, O^{2-}, character. However, for the tricopper species, the spin densities on the μ-oxo atoms differ for $[Cu_3O_3](H_2MOR)$ and $[Cu_3O_3](Na_2MOR)$. For $[Cu_3O_3](H_2MOR)$, there are two μ-oxo sites with significant oxyl characters, spin densities of 0.43 and 0.41 in Table 2. The remaining μ-oxo atom is of oxo O^{2-} character with a spin density of 0.02. In $[Cu_3O_3](Na_2MOR)$, the spin densities on all the μ-oxo atoms are closer to zero. This signifies increased oxo character in the Na-form system. Interestingly, Vogiatzis et al. have reported this anisotropy in the atomic spin densities of the $[Cu_3O_3]^{2+}$ active site.[19] The results in Table 2 suggest that the anisotropy is modified by Na^+ counterions. It will be thus interesting to examine how this effect impacts methane C-H activation.

3.1.3. Structural properties of copper-oxo active sites: The Cu-O_μ bonds within the active site as well as Cu-$O_{framework}$ bond lengths between the active site and framework aluminate oxo atoms are shown in Figure 3. The Cu-Cu bond distances and Cu-O-Cu bond angles are presented in Figure 4. These structural parameters provide a good description of the copper-oxo active sites.

Overall, the Cu-O_μ and Cu-$O_{framework}$ bond lengths of $[Cu_3O_3]^{2+}$ and $[Cu_2O]^{2+}$ are identical in H-MOR and Na-MOR, always within 0.006 Å. The only exception is for $[Cu_3O_3]^{2+}$ in Na-MOR

where the average Cu-$O_{framework}$ bond length is 2.072 Å, about 0.02 Å shorter than in H-MOR, 2.091 Å, Figure 3. The H^+ and Na^+ counter-ions are far-removed from the copper-oxo sites. Thus, it makes sense that the structural properties of the copper-oxo sites are not greatly perturbed by the counter-ions. The Cu-Cu distances are also generally unaffected by the H^+/Na^+ countercation.

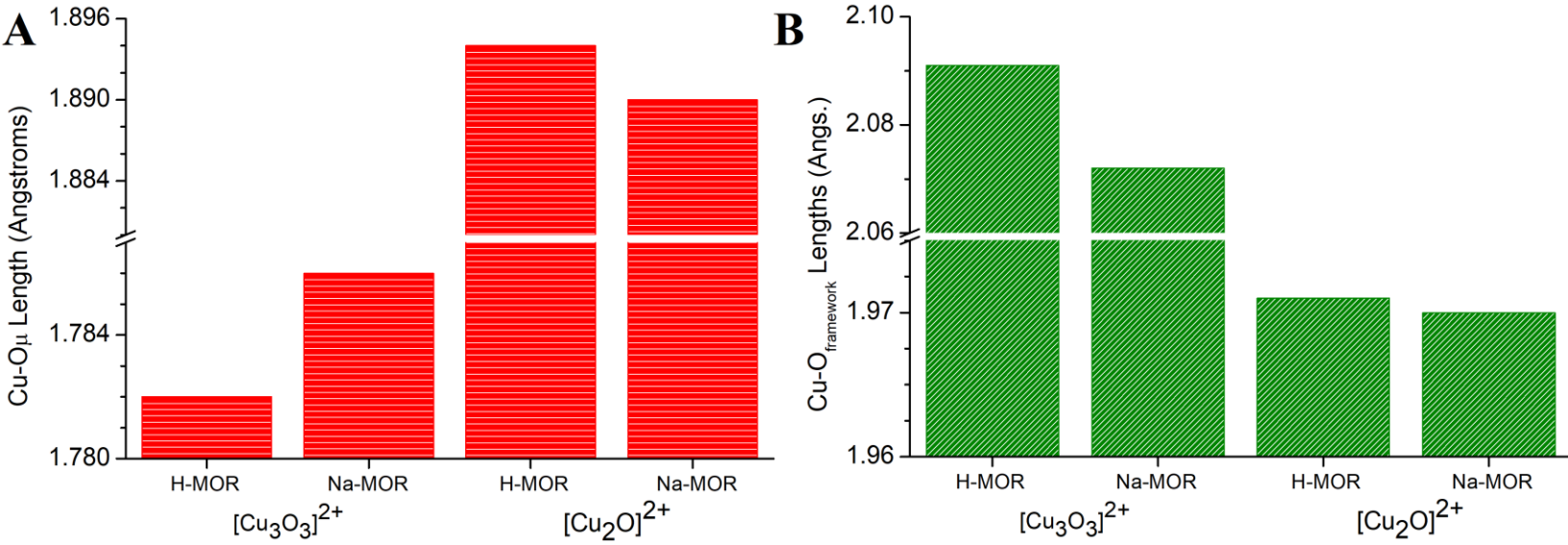

Figure 3: Structural properties of $[Cu_3O_3]^{2+}$ and $[Cu_2O]^{2+}$ in the 8MR of zeolite MOR. **A)** Cu-O_μ bond lengths and **B)** average Cu-$O_{framework}$ distances.

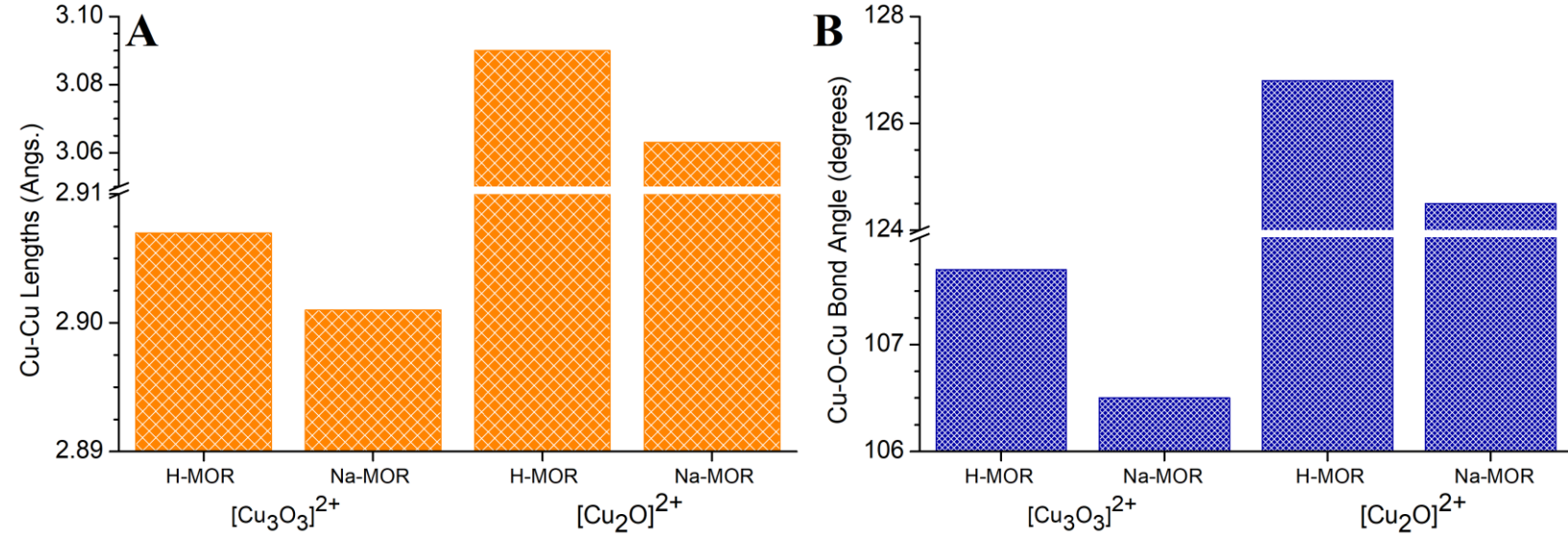

Figure 4: Structural properties of $[Cu_3O_3]^{2+}$ and $[Cu_2O]^{2+}$ in the 8MR of zeolite MOR. **A)** Cu-Cu bond lengths and **B)** average Cu-O-Cu bond angles.

Lastly, the Cu-O-Cu bond angles of $[Cu_3O_3]^{2+}$ and $[Cu_2O]^{2+}$ are reduced by 1.2° and 2.3°, respectively, after replacing H^+ with Na^+, Figure 4. It is however difficult to relate these structural

effects to the differences in the methanol yields and selectivities of H-MOR and Na-MOR zeolites. Overall, we can only speculate that the charge-balancing H^+ or Na^+ ions exert subtle effects on the structure of copper-oxo clusters in the 8MR of MOR. Our findings for $[Cu_3O_3]^{2+}$ and $[Cu_2O]^{2+}$, Table 1 as well Figures 3 and 4, are similar to those of the $[Cu_2O_2]^{2+}$ species.

3.2. Active Site Formation Energies and Temperatures: In this section, we describe the thermodynamics of forming copper-oxo active sites within the 8MR of H-MOR and Na-MOR. The formation reactions for the $[Cu_3O_3]^{2+}$ and $[Cu_2O]^{2+}$ active sites are written as **I-VI**. **I** and **II** are the formation reactions for $[Cu_3O_3]^{2+}$ in H-MOR and Na-MOR, respectively. **III** and **IV** are analogous reactions for formation of $[Cu_2O]^{2+}$. Similar reactions for the $[Cu_2O_2]^{2+}$ species are given in **V** and **VI**. Further discussions are provided in the Supporting Information.

$$3[Cu(H_2O)_6](H_2MOR) + \frac{1}{2}O_2 \rightarrow [Cu_3O_3](H_2MOR) + 2H_4MOR + 16H_2O \quad \textbf{(I)}$$

$$3[Cu(H_2O)_6](Na_2MOR) + \frac{1}{2}O_2 \rightarrow [Cu_3O_3](Na_2MOR) + 2H_2Na_2MOR + 16H_2O \quad \textbf{(II)}$$

$$2[Cu(H_2O)_6](H_2MOR) \rightarrow [Cu_2O](H_2MOR) + H_4MOR + 11H_2O \quad \textbf{(III)}$$

$$2[Cu(H_2O)_6](Na_2MOR) \rightarrow [Cu_2O](Na_2MOR) + H_2Na_2MOR + 11H_2O \quad \textbf{(IV)}$$

$$2[Cu(H_2O)_6](H_2MOR) + \frac{1}{2}O_2 \rightarrow [Cu_2O_2](H_2MOR) + H_4MOR + 11H_2O \quad \textbf{(V)}$$

$$2[Cu(H_2O)_6](Na_2MOR) + \frac{1}{2}O_2 \rightarrow [Cu_2O_2](Na_2MOR) + H_2Na_2MOR + 11H_2O \quad \textbf{(VI)}$$

In **I-VI**, the copper cores of $[Cu(H_2O)_6](H_2MOR)$ and $[Cu(H_2O)_6](Na_2MOR)$, are dehydrated, agglomerated and oxidized. The calculated electronic reaction energies for these reactions are presented in Table 2. The formation energies for the Na-MOR species are generally greater than those of their H-MOR analogues by 5-16 kcal/mol. Also, formation energies for the $[Cu_3O_3]^{2+}$ species are 110-130 kcal/mol higher than for the dicopper species. However, the calculated electronic reaction energies cannot be used to estimate the activation temperatures. For this, we assume that the formation reactions are driven by thermodynamics. This allows us to ignore kinetic effects. We can then estimate the activation temperatures by considering the temperature-dependent reaction free energies, ΔG^T. These are determined by computing the entropy as well as the enthalpy and P-V corrections, a rather expensive proposition for the solids in **I-VI**. We can obtain estimates of the reaction free energies by considering only the corrections for $[Cu(H_2O)_6]^{2+}$ and H_2O, **A** and **B**. **A** applies to the formation of $[Cu_3O_3]^{2+}$ while **B** applies to formation of all the

Table 2: Calculated formation energies and estimated activation temperatures of copper-oxo active sites in the 8MR of H-MOR and Na-MOR.

	Reaction Energy, kcal/mol		Activation Temperature, °C	
Species	H-MOR	Na-MOR	H-MOR	Na-MOR
$[Cu_3O_3]^{2+}$	323.2	330.9	460	484
$[Cu_2O]^{2+}$	205.9	210.4	390	409
Bis(μ-oxo) dicopper (III) $[Cu_2O_2]^{2+}$	195.2	204.6	345	385
Bent μ-(η^2:η^2) peroxo $[Cu_2O_2]^{2+}$	199.8	210.1	363	408

$$\Delta G^T = \Delta E + 3(G-E)_{Cu-aquo\ complex} + 16(G-E)_{water} \qquad \textbf{(A)}$$

$$\Delta G^T = \Delta E + 2(G-E)_{Cu-aquo\ complex} + 11(G-E)_{water} \qquad \textbf{(B)}$$

dicopper active sites. On the reactant side, $[Cu(H_2O)_6]^{2+}$ is considered as being isolated from the framework. The overall free energy corrections, ΔG^T - ΔE, for $[Cu(H_2O)_6]^{2+}$ and H_2O were computed from vibrations in the harmonic approximation. These corrections are shown in Figure 5 and the estimated activation temperatures are presented in Table 2. The free-energy corrections are negative, driving the formation reactions towards exoergicity.

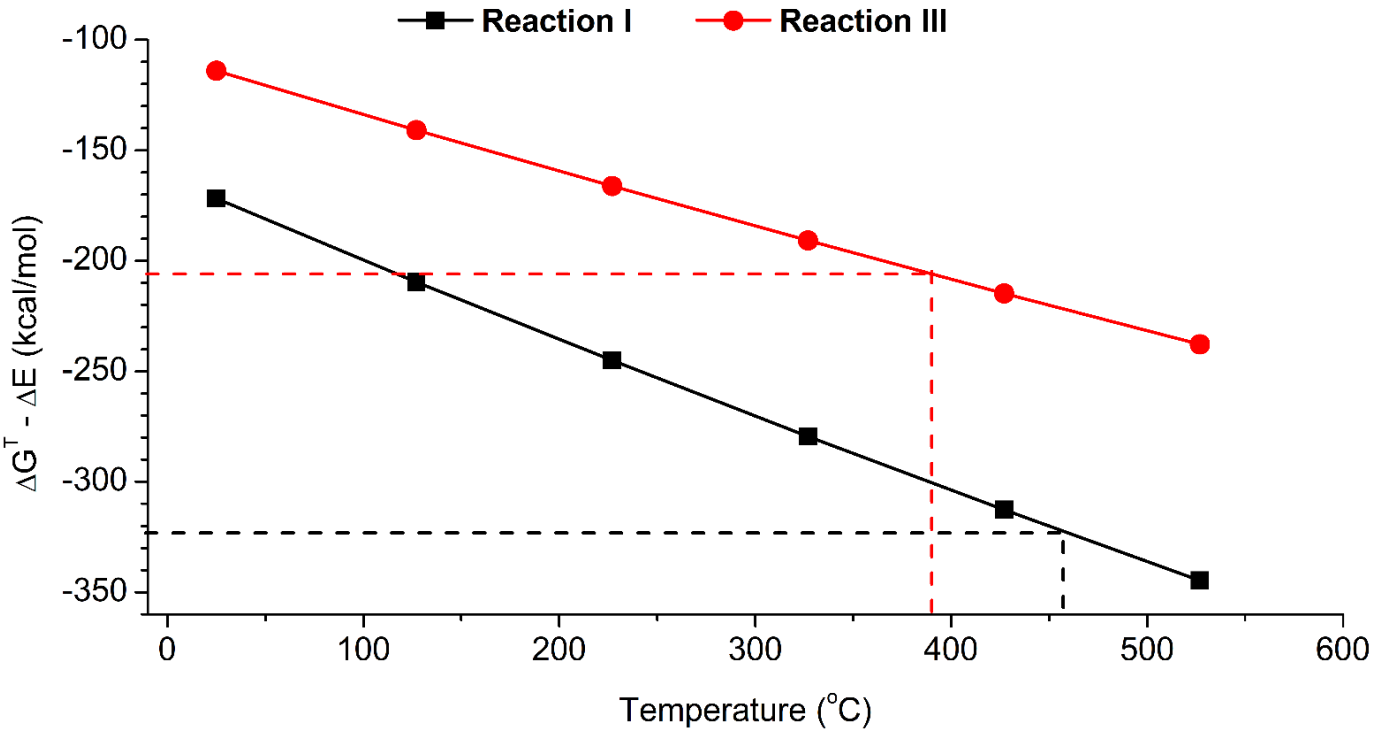

Figure 5: Free-energy corrections, ΔG^T - ΔE, for formation of $[Cu_3O_3]^{2+}$ and $[Cu_2O]^{2+}$ active sites in the 8MR of MOR. The data for $[Cu_2O](H_2MOR)$ and $[Cu_3O_3](H_2MOR)$ are shown.

There are several things to note about the results presented in Figure 5. First, by comparing results in Table 2 and Figure 5, we see that **I-VI** are quite endothermic at room temperature, 25 °C. Therefore, high temperatures are needed to form the copper-oxo clusters, agreeing quite well with experimental protocols. The copper-oxo active sites can be cooled down after formation at high temperatures, as far as the amount of available water is limited, see **I-VI**. Indeed, it is well known that the copper-oxo clusters are highly sensitive to water.[35-38] There are experimental reports indicating that small traces of water in gas lines can reverse changes caused by thermal treatment.[38] Second, the standard entropy of gas-phase water is 188.8 J/mol.K at room temperature.[39] This crudely translates to 72.2 kcal/mol for every 100 °C change in temperature in the case of **A**, just from water. For **B**, this value is 49.6 kcal/mol. These are close to calculated values from vibrational analysis with the harmonic approximation, see Supporting Information.

For $[Cu_3O_3](H_2MOR)$, the free energy approaches 0 kcal/mol only at 460 °C, Table 2. Thus, the temperature needs to be raised to 460 °C before 18 water molecules are removed from 3 unit cells of $[Cu(H_2O)_6](H_2MOR)$, with attendant formation of the $[Cu_3O_3]^{2+}$ site and redox formation of two unit cells of H_4MOR, reaction **I**. This agrees quite well with the experimental protocols usually carried out at 450 °C or even higher temperatures.[13,14,40,41]

The estimated activation temperature of $[Cu_3O_3](Na_2MOR)$ is 484 °C, Table 2. This is quite close to that of $[Cu_3O_3](H_2MOR)$. Indeed the difference of 24 °C between $[Cu_3O_3](H_2MOR)$ and $[Cu_3O_3](Na_2MOR)$ is likely within the accuracy limits of our approach. For producing the dicopper systems, **III-VI**, the activation temperatures in the H-MOR and Na-MOR species differ by 20-50 °C. Table 2 also shows that formation of $[Cu_2O]^{2+}$ is favored at 70 °C below the activation temperatures for $[Cu_3O_3]^{2+}$ in H-MOR. In Na-MOR, the difference between the activation temperatures of $[Cu_2O]^{2+}$ and $[Cu_2O]^{2+}$ is also around 70 °C. Overall, the bis(μ-oxo) dicopper (III) $[Cu_2O_2]^{2+}$ site is more stable than all other sites, Table 2. $[Cu_2O]^{2+}$ is isoenergetic with the bent μ-(η^2:η^2) peroxo $[Cu_2O_2]^{2+}$ site, Table 2. This agrees well with previous DFT results.[42] As such, systems containing the former are also quite likely to contain the latter.

Overall, we conclude that the copper-oxo active sites are formed in the 8MR of H-MOR and Na-MOR around 345-490 °C. $[Cu_3O_3]^{2+}$ is clearly the least stable species, at least relative to the starting $[Cu(H_2O)_6]^{2+}$ species. The bis(μ-oxo) dicopper (III) $[Cu_2O_2]^{2+}$ motif is the most stable and is thus formed at the lowest temperatures. However, the thermodynamics and activation temperatures provide no insights into significant differences between the H-MOR and Na-MOR

zeolites. Differences in the population distributions of the copper-oxo sites in H-MOR and Na-MOR cannot be determined from the thermodynamics of the formation reactions.

3.3. Methane C-H Activation by Copper-Oxo Sites

Here, we examine the transition state barriers for methane C-H bond activation by the copper-oxo active sites of interest. This is important as several experimental reports point to the C-H activation step as the rate-determining step for MMC in several copper-exchanged zeolites.[10,14,43] The calculated barriers are presented in Table S2 of the Supporting Information. The relative energies of all species involved in methane C-H activation are shown in Figure 6. There are several things to note in our results. First, we could not obtain transition states for the bent μ-(η^2:η^2) peroxo active $[Cu_2O_2]^{2+}$ sites. These readily convert to the isoelectronic bis(μ-oxo) dicopper $[Cu_2O_2]^{2+}$ after proton abstraction from methane. We emphasize that this does not preclude the bent μ-(η^2:η^2) peroxo $[Cu_2O_2]^{2+}$ sites from activating methane. We simply were not able to obtain the relevant transition states. Second, the C-H activation barriers on the bis(μ-oxo) dicopper $[Cu_2O_2]^{2+}$ sites are 30.7 and 29.7 kcal/mol in H-MOR and Na-MOR, respectively. These barriers are too high to contribute to methane activation at 200 °C. This is important as methane is often contacted with

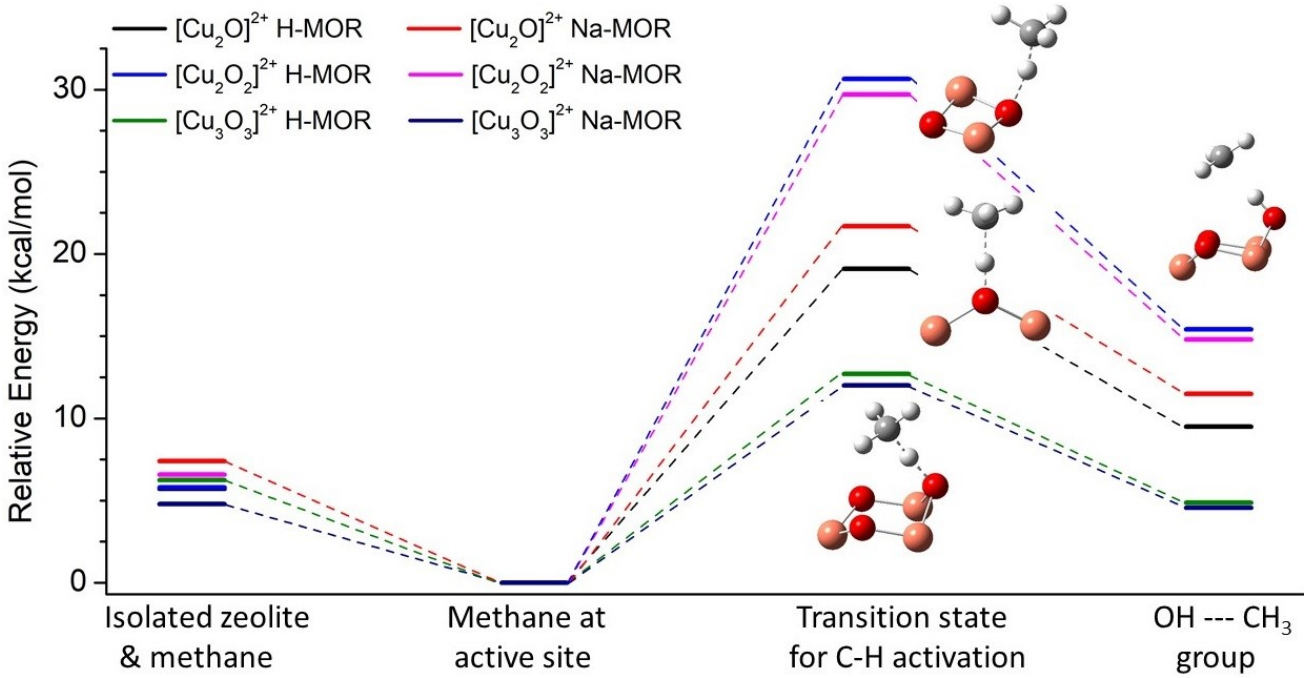

Figure 6: Reaction path for methane activation by $[Cu_3O_3]^{2+}$, bis(μ-oxo) dicopper $[Cu_2O_2]^{2+}$ and $[Cu_2O]^{2+}$ active sites in the 8MR of zeolite MOR with H^+ or Na^+ counter-ions. Barriers at the most reactive oxygen site of $[Cu_3O_3]^{2+}$ are shown.

copper-exchanged zeolites at 200 C in the stepwise MMC process. Turning to $[Cu_2O]^{2+}$, the C-H activation barrier is 21.7 kcal/mol in Na-MOR and 19.1 kcal/mol in H-MOR. Thus, methane can be activated by the $[Cu_2O]^{2+}$ sites at 200 °C. Overall, the transition state is 2.6 kcal/mol higher in Na-MOR than in H-MOR. This is likely close to the accuracy limits of DFT, our structural models as well as the NEB method. Thus, at 200 °C, formation of the methyl intermediates, OH---CH_3 group in Figure 6, likely proceeds in a similar fashion on $[Cu_2O](H_2MOR)$ and $[Cu_2O](Na_2MOR)$. For $[Cu_3O_3]^{2+}$, the C-H activation barriers in H-MOR zeolite are 12.7, 16.0 and 19.0 kcal/mol on the three oxygen atoms. The lowest barrier of 12.7 kcal/mol is found on one of the oxyl sites, Table 2. This is the O(1) site according to the labelling of Vogiatzis et al.[19] The C-H activation barriers at the other oxyl site and the oxo site are comparable. For $[Cu_3O_3](Na_2MOR)$, the barriers are 12.0, 15.1 and 17.7 kcal/mol. The barriers at O(1) are comparable for $[Cu_3O_3](Na_2MOR)$ and $[Cu_3O_3](Na_2MOR)$. Thus, the C-H activation barriers follow the trend $[Cu_3O_3](Na_2MOR) \sim [Cu_3O_3](H_2MOR) < [Cu_2O](H_2MOR) \sim [Cu_2O](Na_2MOR) <<< [Cu_2O_2](Na_2MOR) \sim [Cu_2O_2](H_2MOR)$. This trend provides no insights into the different methanol yields and selectivities for H-MOR and Na-MOR zeolites.

3.4. Fate of Methyl Group from Methane

The methyl group formed from methane C-H bond activation is fairly unstable relative to the starting adduct complex, Figure 6. To stabilize the whole system, this methyl group can rebound to other portions of the active site and zeolite. As a matter of fact, the system can be greatly stabilized if the methyl group rebounds to a μ-oxo atom of a copper-oxo active site. For $[Cu_2O]^{2+}$, this corresponds to [Cu-(OCH_3)-Cu] and [Cu-(OH)-Cu] intermediates. These were proposed previously by Alayon et al.[36] For $[Cu_3O_3]^{2+}$, the methyl can rebound to the same site forming a $[Cu_3(\mu\text{-}OCH_3)(\mu\text{-}OH)(\mu\text{-}O)]^{2+}$ intermediate, which is also very stable. The energies of these intermediates are given relative to the methane-adduct complex in Figure 7. Intermediates with μ-(OCH_3) character are significantly more stable than situations in which the methyl group rebounds to a copper center.

Interestingly, after methane C-H activation and rebound of the methyl group to the active site, there are two additional electrons in the copper-oxo clusters. This is because methane activation is associated with the Cu^{2+}/Cu^{+} redox couple in $[Cu_2O]^{2+}$. Simply, electrons are transferred from methane to copper center(s). We recently used electronic structure analysis of several intra-zeolite

surface methoxy species to show that methane activation in $[Cu_3O_3]^{2+}$ is due to an interesting combination of the Cu^{2+}/Cu^{+} and O^{-}/O^{2-} redox couples.[44] Simply, an electron is transferred from methane to a copper site and another reduces an oxyl. Thus, positioning the methyl group near the electron-rich copper-oxo cores would create opportunities for over-oxidation. In Figure 8, we show that a proton is readily transferred from the μ-(OCH_3) group to a μ-oxo atom of $[Cu_3O_3](H_2MOR)$.

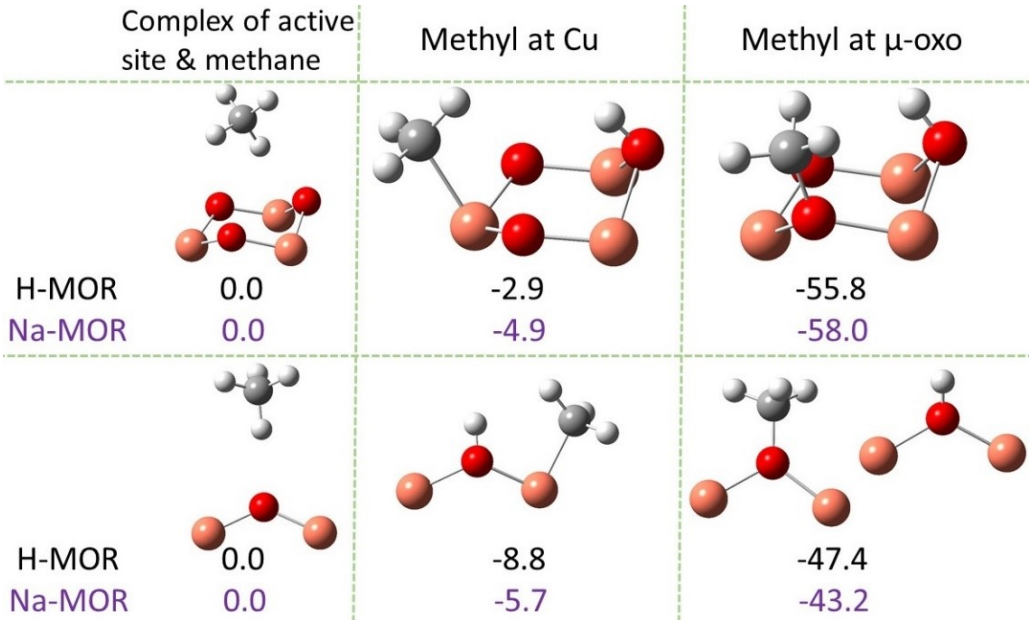

Figure 7: Relative energies, in kcal/mol, of possible intermediates from rebound of the methyl group formed during methane C-H activation.

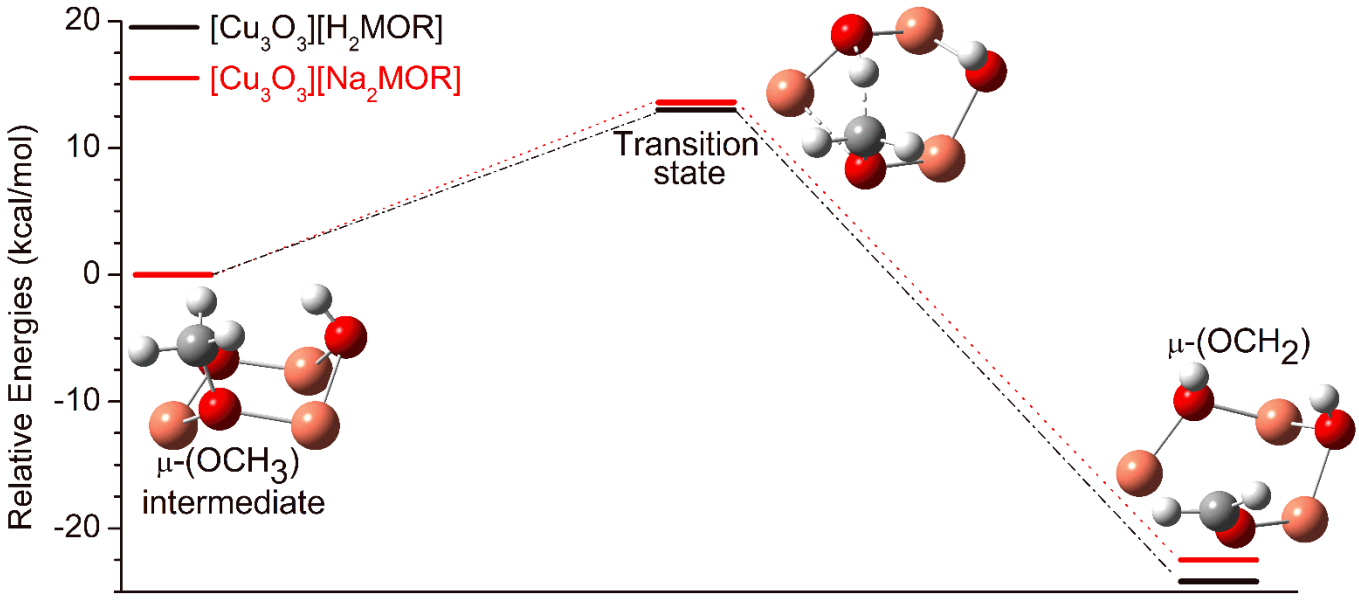

Figure 8: Transfer of a proton from the μ-(OCH_3) group as the beginning of over-oxidation at the active sites of $[Cu_3O_3](H_2MOR)$ and of $[Cu_3O_3](Na_2MOR)$.

The barrier for this proton transfer is quite low, only 13.0 kcal/mol at the periodic PBE-D3 level. A similar barrier, 13.6 kcal/mol, was obtained for $[Cu_3O_3](Na_2MOR)$, Figure 8. We confirmed that the C-H bond was elongated to 1.340-1.344 Å at the transition states. Also, the magnitudes of the transition state barriers indicates that these processes are quite facile at 200 °C. These proton transfer steps are also strongly exothermic and lead to the formation of a μ-($O{=}CH_2$) group. This is a likely precursor for carbon monoxide and other over-oxidation products. As such, methanol selectivity is ensured only when the methyl group is stabilized at a location remote from the electron-rich active sites. The μ-($O{=}CH_2$) moiety is adsorbed formaldehyde. Sushkevich et al. recently reported the presence of formaldehyde during activation of methane by extra-framework Cu^{2+}-based active sites in zeolites.[45]

Interestingly, copper-exchanged zeolites contain aluminate tetrahedra in H_4MOR and Na_4MOR systems, Figure 1. Thus, one possibility of stabilizing the methyl group would be to transfer it from the copper-oxo active site to a remote H_4MOR or Na_4MOR unit cell, in exchange for H^+ or Na^+, respectively. This is illustrated for $[Cu_3O_3](H_2MOR)$ in **VII** and for $[Cu_3O_3](Na_2MOR)$ in **VIII**. Indeed, framework aluminate groups have been previously suggested as possible sites for stabilizing the separated methyl groups formed during methane activation.

$$[Cu_3O_3](CH_4)(H_2MOR) + H_4MOR \rightarrow [Cu_3(\mu-OH)_2(\mu-O)](H_2MOR) + H_3(CH_3)MOR \quad (\textbf{VII})$$

$$[Cu_3O_3](CH_4)(Na_2MOR) + Na_4MOR \rightarrow [Cu_3(\mu-ONa)_2(\mu-O)](Na_2MOR) + Na_3(CH_3)MOR \quad (\textbf{VII})$$

$[Cu_3O_3](CH_4)(H_2MOR)$ and $[Cu_3O_3](CH_4)(Na_2MOR)$ are the adduct complexes of methane and the copper-oxo site. $H_3(CH_3)MOR$ and $Na_3(CH_3)MOR$ are formed after exchange of H^+/Na^+ from H_4MOR/Na_4MOR with the methyl group of activated methane. $[Cu_3(\mu-OH)_2(\mu-O)](H_2MOR)$ and $[Cu_3(\mu-ONa)_2(\mu-O)](H_2MOR)$ have μ-(OH) and μ-(ONa) groups, respectively, at the active site rather than a μ-(OCH_3) moiety. We emphasize again that there are four aluminate groups in H_4MOR. Simply **VII**-**VIII** shows that the separated methyl group formed from methane activation is stabilized at one of the framework aluminates of H_4MOR. The methyl group is exchanged for H^+ or Na^+. **VII**-**VIII** indicate that activation of the methane C-H bond at the copper-oxo active site facilitates exchange with framework H^+ or Na^+ sites. This conforms with the finding of Gabrienko et al.[46] Crucially, species formed from stabilizing the methyl group in remote H_4MOR and Na_4MOR unit cells must be as stable as the μ-(OCH_3)-stabilized intermediates we

initially considered, Figure 7. Failing this, the μ-(OCH_3)-stabilized intermediates are preferred and over-oxidation increases, Figure 8. The relative energies for stabilizing the methyl group at remote aluminate tetrahedra of H_4MOR and Na_4MOR, **VII**, are presented in Table 4.

For $[Cu_2O](H_2MOR)$ and $[Cu_3O_3](H_2MOR)$, the methyl group stabilized at the aluminate of H_4MOR are respectively stable by -44.3 and -51.8 kcal/mol. These energies are relative to the adduct complexes of the oxo site with methane. Also, these values are to be compared with -47.4 and -55.8 kcal/mol for the μ-(OCH_3)-stabilized intermediates, Table 4 and Figure 7. Therefore, stabilization at remote aluminate tetrahedra, via exchange of a methyl with H^+, is energetically close to stabilization at μ-oxo sites. We conclude that BASs are crucial for stabilizing the methyl group, away from over-oxidation at the copper-oxo sites. NMR spectroscopic measurements have been used to confirm location of surface methoxy groups at zeolite BASs.[47,48] Indeed, work by Kolganov et al. and Sushkevich et al. clearly indicate that the separated methyl group can be stabilized at BASs.[45,49,50] Sushkevich et al. concluded that methoxy groups bound to BAS is one of the main products formed over Cu-MOR with a Si/Al ratio of 6. This is close to the ratio of 11 for our model systems. Indeed, our results in Table 4 show that the copper oxo sites catalyze exchange of the methyl group of methane with the BASs. It would also be reasonable to expect that the protons of methane can be readily exchanged with BASs, in the presence of the copper-oxo species. This is exactly the findings of Gabrienko et al.[46]

Table 4: Calculated stabilization energies, kcal/mol, due to rebound of methyl group to a copper atom, an active site μ-oxo group or to remote aluminate tetrahedra of H_4MOR or Na_4MOR.

	Cu	μ-(OCH_3)	Aluminate of H_4MOR	Aluminate of Na_4MOR
$[Cu_3O_3](H_2MOR)$	-2.9	-55.8	-51.8	
$[Cu_3O_3](Na_2MOR)$	-4.9	-58.0	-54.5	-35.4
$[Cu_2O](H_2MOR)$	-8.8	-47.4	-44.3	
$[Cu_2O](Na_2MOR)$	-5.7	-43.2	-40.6	-27.2

Exchange of the methyl group with a remote Na^+ from Na_4MOR stabilizes $[Cu_2O](Na_2MOR)$ and $[Cu_3O_3](Na_2MOR)$ by -27.2 and -35.4 kcal/mol, respectively, Table 4. These are far less than the energies of the μ-(OCH_3)-stabilized intermediates for these species, -43.2 and -58.0 kcal/mol, respectively, Table 4. The over-oxidation route via the μ-(OCH_3) group thus prevails. Simply speaking, Na^+ prefers to bind to aluminate tetrahedra rather than help stabilize the methyl group at these locations. We earlier described the electronic structure basis for this preference, Table 1. It is

reasonable to expect that these trends would extend to octahedral aluminum species. Na^+ simply prefers ionic coordination to aluminum-oxo species rather than help stabilize the active site and the methyl group from methane.

Interestingly for $[Cu_2O](Na_2MOR)$ and $[Cu_3O_3](Na_2MOR)$, we can also consider that BASs are present as H_4MOR. In that situation, the methyl group from methane can be exchanged with a proton from H_4MOR rather than with Na^+ from Na_4MOR. In Table 4, we see that the methyl-proton exchange stabilizes the $[Cu_2O](Na_2MOR)$ and $[Cu_3O_3](Na_2MOR)$ systems by -40.6 and -54.5 kcal/mol, respectively. These are significantly much closer to the stabilization energies of the μ-(OCH_3) intermediates. Thus, Na-MOR systems can also avoid over-oxidation when the methyl group from methane is stabilized at a remote BAS. Methanol yield and selectivity are thus clearly correlated to the concentration of BASs.[9,12,13,16] For systems containing both Na^+ and H^+ counter-ions, greater methanol yields and selectivities will be obtained with higher concentrations of BASs.

CONCLUSIONS

In this work, we used periodic density functional theory (DFT) to analyze the electronic structure properties, formation and reactivities of several copper-oxo species in sodium-form and proton-form zeolites. These copper-oxo active sites are interesting due to their abilities to activate methane to methanol. Specifically, we investigated the properties of $[Cu_2O]^{2+}$, $[Cu_2O_2]^{2+}$, and $[Cu_3O_3]^{2+}$ active sites in the 8-membered ring, 8MR, of zeolite mordenite, MOR, with proton or sodium counter-ions, Na-MOR or H-MOR. DFT calculations were to probe how the counter-ions perturb the active site geometries and electronic structures. The influence of the counter-ions on the activation temperatures of the active sites was also investigated. Lastly, we examined how the counter-ions affect the methane C-H activation process as well as the fate of the methyl group produced from this process. We sought to use insights from these investigations to quantitatively explain observations of higher methanol yields and selectivities in zeolites with proton precursors. Overall, we have found that:

1) The active site geometries are quite similar in the Na-MOR and H-MOR zeolites. This is due to the fact that the counter-ions are far-removed from the copper-oxo clusters. However, the frameworks are significantly more nucleophilic in the Na-MOR systems than analogous H-MOR species.

2) The activation temperatures of the copper-oxo active sites were predicted by considering the reaction energies for dehydrating and oxidizing $[Cu(H_2O)_6]^{2+}$ complexes. Subsequently, a simple scheme for obtaining temperature-dependent free-energy corrections allows us to estimate their activation temperatures. The active sites are formed at 345-490 °C. The bis(μ-oxo) dicopper (III) $[Cu_2O_2]^{2+}$ species are formed at the lowest temperatures while tricopper $[Cu_3O_3]^{2+}$ sites are formed at the highest temperatures. Specifically, the estimated activation temperature for $[Cu_3O_3]^{2+}$ in H-MOR is 460 °C. This agrees with experimental protocols at 450 °C. Overall, the thermodynamics of forming the copper-oxo clusters provide little insights into how H^+/Na^+ counter-ions affect the population distribution and reactivities of the active sites.
3) $[Cu_2O]^{2+}$ and $[Cu_3O_3]^{2+}$ cores are able to activate methane at 200 °C. However, the C-H activation barriers are largely similar in the H-MOR and Na-MOR zeolites. The separated methyl group formed from C-H activation is however relatively unstable. To lower the overall energies of the systems, this methyl group needs to be stabilized.
4) There are various ways to stabilize the methyl group. One such opportunity involves rebound to a μ-oxo atom of the active site cluster. This stabilizes the overall system by 40-60 kcal/mol. This is the case for $[Cu_2O]^{2+}$ and $[Cu_3O_3]^{2+}$. Interestingly, the μ-(OCH_3) groups formed from this rebound are reactive. They can readily transfer a proton to another μ-oxo atom, resulting in the formation of μ-($O{=}CH_2$). Recent spectroscopic investigations have identified the CH_2O group (as adsorbed formaldehyde) as an intermediate in the formation of over-oxidation products like CO. The barriers for this transfer are about 13-14 kcal/mol. The transfer is also strongly exothermic. Clearly, the μ-($O{=}CH_2$) group is a precursor for over-oxidation products. Thus, stabilization of the methyl group at μ-oxo atoms of the copper-oxo clusters is a pathway to over-oxidation.
5) To avoid over-oxidation, the methyl group must be stabilized at a remote location, far removed from the electron-rich active sites. We considered remote aluminate tetrahedra with H^+ and Na^+ counter-ions as optimal locations for this stabilization. In H-MOR systems, exchange of the methyl group with H^+ provides structures that are as stable as the μ-(OCH_3)-stabilized intermediates. Thus by stabilizing at remote Brønsted acid sites, these systems are able to avoid over-oxidation. This conforms to recent reports that show the copper-oxo sites facilitate proton exchange between methane and Brønsted acid sites. However, in Na-MOR species, exchange

of the methyl group with remote Na^+ provides significantly less stabilization than the μ-(OCH_3) intermediates. Thus, over-oxidation will be important for Na-MOR species. Interestingly, exchange of the methyl group in Na-MOR systems with remote Brønsted acid sites restores near-parity with the μ-(OCH_3)-stabilized intermediates. This explains why methanol yields and selectivities depend crucially on the concentrations of Brønsted acid sites.

■ ASSOCIATED CONTENT

Supporting Information.

The Supporting Information is available free of charge via the Internet at http://pubs.acs.org.

Optimized geometries and energies of all systems considered in this work.

■ AUTHOR INFORMATION

Corresponding Authors

*S.O.O.: E-mail: sodoh@unr.edu

Notes

[#]These authors participated equally to this work.

The authors declare no competing financial interest.

■ ACKNOWLEDGMENT

This material is based upon work supported by the National Science Foundation under Grant No. 1800387.

■ REFERENCES

(1) Dunn, S. Hydrogen futures: toward a sustainable energy system. *International Journal of Hydrogen Energy* **2002**, *27*, 235.

(2) Lunsford, J. H. Catalytic conversion of methane to more useful chemicals and fuels: a challenge for the 21st century. *Catalysis Today* **2000**, *63*, 165.

(3) Muradov, N. Z.; Veziroglu, T. N. From hydrocarbon to hydrogen-carbon to hydrogen economy. *International Journal of Hydrogen Energy* **2005**, *30*, 225.

(4) Wang, Q.; Chen, X.; Jha, A. N.; Rogers, H. Natural gas from shale formation - The evolution, evidences and challenges of shale gas revolution in United States. *Renewable & Sustainable Energy Reviews* **2014**, *30*, 1.

(5) Dandu, N. K.; Reed, J. A.; Odoh, S. O. Performance of Density Functional Theory for Predicting Methane-to-Methanol Conversion by a Tri-Copper Complex. *J. Phys. Chem. C* **2018**, *122*, 1024.

(6) Ipek, B.; Wulfers, M. J.; Kim, H.; Goltl, F.; Hermans, I.; Smith, J. P.; Booksh, K. S.; Brown, C. M.; Lobo, R. F. Formation of $Cu_2O_2^{2+}$ and Cu_2O^{2+} toward C-H Bond Activation in Cu-SSZ-13 and Cu-SSZ-39. *ACS Catal.* **2017**, *7*, 4291.

(7) Kulkarni, A. R.; Zhao, Z. J.; Siahrostami, S.; Norskov, J. K.; Studt, F. Cation-exchanged zeolites for the selective oxidation of methane to methanol. *Catalysis Science & Technology* **2018**, *8*, 114.

(8) Li, G. N.; Vassilev, P.; Sanchez-Sanchez, M.; Lercher, J. A.; Hensen, E. J. M.; Pidko, E. A. Stability and reactivity of copper oxo-clusters in ZSM-5 zeolite for selective methane oxidation to methanol. *Journal of Catalysis* **2016**, *338*, 305.

(9) Park, M. B.; Park, E. D.; Ahn, W. S. Recent Progress in Direct Conversion of Methane to Methanol Over Copper-Exchanged Zeolites. *Frontiers in Chemistry* **2019**, *7*, 514.

(10) Snyder, B. E. R.; Bols, M. L.; Schoonheydt, R. A.; Sels, B. F.; Solomon, E. I. Iron and Copper Active Sites in Zeolites and Their Correlation to Metalloenzymes. *Chem. Rev.* **2018**, *118*, 2718.

(11) Newton, M. A.; Knorpp, A. J.; Sushkevich, V. L.; Palagin, D.; van Bokhoven, J. A. Active sites and mechanisms in the direct conversion of methane to methanol using Cu in zeolitic hosts: a critical examination. *Chem. Soc. Rev.* **2020**, *49*, 1449.

(12) Dyballa, M.; Pappas, D. K.; Kvande, K.; Borfecchia, E.; Arstad, B.; Beato, P.; Olsbye, U.; Svelle, S. On How Copper Mordenite Properties Govern the Framework Stability and Activity in the Methane-to-Methanol Conversion. *ACS Catal.* **2019**, *9*, 365.

(13) Grundner, S.; Luo, W.; Sanchez-Sanchez, M.; Lercher, J. A. Synthesis of single-site copper catalysts for methane partial oxidation. *Chemical Communications* **2016**, *52*, 2553.

(14) Grundner, S.; Markovits, M. A. C.; Li, G.; Tromp, M.; Pidko, E. A.; Hensen, E. J. M.; Jentys, A.; Sanchez-Sanchez, M.; Lercher, J. A. Single-site trinuclear copper oxygen clusters in mordenite for selective conversion of methane to methanol. *Nat. Commun.* **2015**, *6*, 7546.

(15) Narsimhan, K.; Iyoki, K.; Dinh, K.; Roman-Leshkov, Y. Catalytic Oxidation of Methane into Methanol over Copper-Exchanged Zeolites with Oxygen at Low Temperature. *ACS Cent. Sci.* **2016**, *2*, 424.

(16) Sushkevich, V. L.; van Bokhoven, J. A. Effect of Brønsted acid sites on the direct conversion of methane into methanol over copper-exchanged mordenite. *Catalysis Science & Technology* **2018**, *8*, 4141.

(17) Park, M. B.; Ahn, S. H.; Mansouri, A.; Ranocchiari, M.; van Bokhoven, J. A. Comparative Study of Diverse Copper Zeolites for the Conversion of Methane into Methanol. *ChemCatChem* **2017**, *9*, 3705.

(18) Narsimhan, K.; Michaelis, V. K.; Mathies, G.; Gunther, W. R.; Griffin, R. G.; Román-Leshkov, Y. Methane to Acetic Acid over Cu-Exchanged Zeolites: Mechanistic Insights from a Site-Specific Carbonylation Reaction. *J. Am. Chem. Soc.* **2015**, *137*, 1825.

(19) Vogiatzis, K. D.; Li, G. N.; Hensen, E. J. M.; Gagliardi, L.; Pidko, E. A. Electronic Structure of the $[Cu_3(\mu\text{-}O)_3]^{2+}$ Cluster in Mordenite Zeolite and Its Effects on the Methane to Methanol Oxidation. *J. Phys. Chem. C* **2017**, *121*, 22295.

(20) Giannozzi, P.; Baroni, S.; Bonini, N.; Calandra, M.; Car, R.; Cavazzoni, C.; Ceresoli, D.; Chiarotti, G. L.; Cococcioni, M.; Dabo, I. *et al.* QUANTUM ESPRESSO: a modular and open-source software project for quantum simulations of materials. *Journal of Physics: Condensed Matter* **2009**, *21*, 395502.

(21) Giannozzi, P.; Andreussi, O.; Brumme, T.; Bunau, O.; Buongiorno Nardelli, M.; Calandra, M.; Car, R.; Cavazzoni, C.; Ceresoli, D.; Cococcioni, M. *et al.* Advanced capabilities for materials modelling with Quantum ESPRESSO. *Journal of Physics: Condensed Matter* **2017**, *29*, 465901.

(22) Grimme, S.; Ehrlich, S.; Goerigk, L. Effect of the damping function in dispersion corrected density functional theory. *Journal of Computational Chemistry* **2011**, *32*, 1456.

(23) Perdew, J. P.; Burke, K.; Ernzerhof, M. Generalized Gradient Approximation Made Simple. *Phys. Rev. Lett.* **1996**, *77*, 3865.

(24) VandeVondele, J.; Krack, M.; Mohamed, F.; Parrinello, M.; Chassaing, T.; Hutter, J. Quickstep: Fast and accurate density functional calculations using a mixed Gaussian and plane waves approach. *Computer Physics Communications* **2005**, *167*, 103.

(25) Kühne, T. D.; Iannuzzi, M.; Ben, M. D.; Rybkin, V. V.; Seewald, P.; Stein, F.; Laino, T.; Khaliullin, R. Z.; Schütt, O.; Schiffmann, F. *et al.* CP2K: An electronic structure and molecular dynamics

software package - Quickstep: Efficient and accurate electronic structure calculations. *J. Chem. Phys.* **2020**, *152*, 194103.

(26) VandeVondele, J.; Hutter, J. An efficient orbital transformation method for electronic structure calculations. *J. Chem. Phys.* **2003**, *118*, 4365.

(27) VandeVondele, J.; Hutter, J. Gaussian basis sets for accurate calculations on molecular systems in gas and condensed phases. *J. Chem. Phys.* **2007**, *127*, 114105.

(28) Goedecker, S.; Teter, M.; Hutter, J. Separable dual-space Gaussian pseudopotentials. *Phys. Rev. B* **1996**, *54*, 1703.

(29) Hartwigsen, C.; Goedecker, S.; Hutter, J. Relativistic separable dual-space Gaussian pseudopotentials from H to Rn. *Phys. Rev. B* **1998**, *58*, 3641.

(30) VandeVondele, J.; Hutter, J. Gaussian Basis Sets for Accurate Calculations on Molecular Systems in Gas and Condensed Phases. *J. Chem. Phys.* **2007**, *127*, 114105.

(31) Hirshfeld, F. L. Bonded-atom fragments for describing molecular charge densities. *Theoretica chimica acta* **1977**, *44*, 129.

(32) Jonsson, H.; MillS, G.; Jacobsen, K. W. In *Classical and Quantum Dynamics in Condensed Phase Simulations*, p 385.

(33) Mills, G.; Jónsson, H. Quantum and thermal effects in ${\mathrm{H}}_{2}$ dissociative adsorption: Evaluation of free energy barriers in multidimensional quantum systems. *Phys. Rev. Lett.* **1994**, *72*, 1124.

(34) Aprà, E.; Bylaska, E. J.; de Jong, W. A.; Govind, N.; Kowalski, K.; Straatsma, T. P.; Valiev, M.; van Dam, H. J. J.; Alexeev, Y.; Anchell, J. *et al.* NWChem: Past, present, and future. *J. Chem. Phys.* **2020**, *152*, 184102.

(35) Sushkevich, V. L.; van Bokhoven, J. A. Kinetic study and effect of water on methane oxidation to methanol over copper-exchanged mordenite. *Catalysis Science & Technology* **2020**, *10*, 382.

(36) Alayon, E. M. C.; Nachtegaal, M.; Bodi, A.; van Bokhoven, J. A. Reaction Conditions of Methane-to-Methanol Conversion Affect the Structure of Active Copper Sites. *ACS Catal.* **2014**, *4*, 16.

(37) Ikuno, T.; Grundner, S.; Jentys, A.; Li, G. N.; Pidko, E.; Fulton, J.; Sanchez-Sanchez, M.; Lercher, J. A. Formation of Active Cu-oxo Clusters for Methane Oxidation in Cu-Exchanged Mordenite. *J. Phys. Chem. C* **2019**, *123*, 8759.

(38) Ikuno, T.; Sanchez-Sanchez, M. In *https://dechema.de/-p-20083435-EGOTEC-11b007e7025759b4bf756543a9acead4/_/3568_Schlussbericht.pdf;* Vol. 2021.

(39) Franck, E. U. J. D. Cox, D. D. Wagman, V. A. Medvedev: CODATA — Key Values for Thermodynamics, aus der Reihe: CODATA, Series on Thermodynamic Properties. Hemisphere Publishing Corporation, New York, Washington, Philadelphia, London 1989. 271 Seiten, Preis: £ 28.00. *Berichte der Bunsengesellschaft für physikalische Chemie* **1990**, *94*, 93.

(40) Kim, Y.; Kim, T. Y.; Lee, H.; Yi, J. Distinct activation of Cu-MOR for direct oxidation of methane to methanol. *Chemical Communications* **2017**, *53*, 4116.

(41) Le, H. V.; Parishan, S.; Sagaltchik, A.; Göbel, C.; Schlesiger, C.; Malzer, W.; Trunschke, A.; Schomäcker, R.; Thomas, A. Solid-State Ion-Exchanged Cu/Mordenite Catalysts for the Direct Conversion of Methane to Methanol. *ACS Catal.* **2017**, *7*, 1403.

(42) Goodman, B. R.; Hass, K. C.; Schneider, W. F.; Adams, J. B. Cluster Model Studies of Oxygen-Bridged Cu Pairs in Cu−ZSM-5 Catalysts. *J. Phys. Chem. B* **1999**, *103*, 10452.

(43) Woertink, J. S.; Smeets, P. J.; Groothaert, M. H.; Vance, M. A.; Sels, B. F.; Schoonheydt, R. A.; Solomon, E. I. A Cu_2O^{2+} core in Cu-ZSM-5, the active site in the oxidation of methane to methanol. *Proceedings of the National Academy of Sciences of the United States of America* **2009**, *106*, 18908.

(44) Suleiman, O.; Panthi, D.; Adeyiga, O.; Odoh, S. O. Methane C-H Activation by $[Cu_2O]^{2+}$ and $[Cu_3O_3]^{2+}$ in Copper-Exchanged Zeolites: Computational Analysis of Redox Chemistry and X-ray Absorption Spectroscopy. *Inorg. Chem.* **2021**, submitted.

(45) Sushkevich, V. L.; Verel, R.; van Bokhoven, J. A. Pathways of Methane Transformation over Copper-Exchanged Mordenite as Revealed by In Situ NMR and IR Spectroscopy. *Angew. Chem. Int. Edit.* **2020**, *59*, 910.

(46) Gabrienko, A. A.; Kolganov, A. A.; Arzumanov, S. S.; Yashnik, S. A.; Kriventsov, V. V.; Freude, D.; Stepanov, A. G. Effect of Copper State in Cu/H-ZSM-5 on Methane Activation by Brønsted Acid Sites, Studied by 1H MAS NMR In Situ Monitoring the H/D Hydrogen Exchange of the Alkane with Brønsted Acid Sites. *J. Phys. Chem. C* **2021**, *125*, 2182.

(47) Dyballa, M.; Thorshaug, K.; Pappas, D. K.; Borfecchia, E.; Kvande, K.; Bordiga, S.; Berlier, G.; Lazzarini, A.; Olsbye, U.; Beato, P. *et al.* Zeolite Surface Methoxy Groups as Key Intermediates in the Stepwise Conversion of Methane to Methanol. *Chemcatchem* **2019**, *11*, 5022.

(48) Zheng, J.; Lee, I.; Khramenkova, E.; Wang, M.; Peng, B.; Gutierrez, O. Y.; Fulton, J. L.; Camaioni, D. M.; Khare, R.; Jentys, A. *et al.* Importance of Methane Chemical Potential for Its Conversion to Methanol on Cu-Exchanged Mordenite. *Chemistry-a European Journal* **2020**, *26*, 7563.

(49) Kolganov, A. A.; Gabrienko, A. A.; Chernyshov, I. Y.; Stepanov, A. G.; Pidko, E. A. The accuracy challenge of the DFT-based molecular assignment of C-13 MAS NMR characterization of surface intermediates in zeolite catalysis. *Phys. Chem. Chem. Phys.* **2020**, *22*, 24004.

(50) Kolganov, A. A.; Gabrienko, A. A.; Yashnik, S. A.; Pidko, E. A.; Stepanov, A. G. Nature of the Surface Intermediates Formed from Methane on Cu-ZSM-5 Zeolite: A Combined Solid-State Nuclear Magnetic Resonance and Density Functional Theory Study. *J. Phys. Chem. C* **2020**, *124*, 6242.

For Table of Contents Only